TECHNICAL TRANSACTIONS | CZASOPISMO TECHNICZNE
MECHANICS | MECHANIKA
2-M/2015

MARCIN HOJNY*, JACEK TARASIUK**, SEBASTIAN WROŃSKI**

DEVELOPMENT OF THE MODELING STRATEGY FOR THE STEEL DEFORMATION IN SEMI-SOLID STATE – TOMOGRAPHIC STUDIES

OPRACOWANIE KOMPLEKSOWEGO PODEJŚCIA DO MODELOWANIA ODKSZTAŁCANIA STALI W STANIE PÓŁCIEKŁYM – BADANIA TOMOGRAFICZNE

Abstract

The condition of steel deformation in a semi-solid state should be as isothermal as possible due to the very high sensitivity of material rheology to even small variations of temperature. The basic reason for uneven temperature distribution (melting zone) inside the sample body on the Gleeble thermo-mechanical simulator is the contact with cold/warm copper handles. The semi-solid conditions in central parts of the sample cause even greater temperature gradient due to latent transformation heat. Such non-uniform temperature distribution is the source of significant differences in the microstructure and, hence, in material rheological properties. In the paper example results of tomographic studies were presented for both experimental variants (with warm and cold handles).

Keywords: *physical simulation, computer tomography, extra-high temperatures*

Streszczenie

Proces odkształcania stali w stanie półciekłym powinien być realizowany w warunkach izotermicznych, w związku z dużą czułością własności mechanicznych na niewielkie zmiany temperatury. Głównym powodem nierównomiernego rozkładu temperatury (kształtu strefy przetopienia) w objętości próbki jest wpływ użytych podczas eksperymentów uchwytów miedzianych, tzw. ciepłych i zimnych. Kolejnym ważnym czynnikiem wpływającym na kształt strefy przetopienia jest generowane ciepło krzepnięcia wpływające także bezpośrednio na kształt strefy przetopienia i właściwości mikrostrukturalne i reologiczne. W prezentowanej pracy przedstawiono przykładowe wyniki analiz tomograficznych dla dwóch próbek, z których każda była przetapiana w innej konfiguracji narzędzi (uchwyty zimne i ciepłe).

Słowa kluczowe: *symulacja fizyczna, tomografia komputerowa, wysokie temperatury*

* Ph.D. Marcin Hojny, Faculty of Metals Engineering and Industrial Computer Science, AGH University of Science and Technology.

** Ph.D. D.Sc. Eng. Jacek Tarasiuk, Ph.D. Sebastian Wroński, Faculty of Physics and Applied Computer Science, AGH University of Science and Technology.

1. Introduction

The physical simulations of the melting process were done in the Institute for Ferrous Metallurgy in Gliwice, Poland, using a Gleeble 3800 thermo-mechanical simulator. The steel used for the experiments was the C45 grade steel with 0.45% carbon content. During the experiments samples were heated to 1430°C and after being maintained at a constant temperature they were cooled down. More details about physical and computer simulations of steel deformations in a semi-solid state can be found in [6].

The micro tomography measurements presented in this paper were performed using a "nanotom 180N" device produced by GE Sensing & Inspection Technologies phoenix|X-ray Gmbh. The machine is equipped with a nanofocus X-ray tube with a maximum of 180kV voltage. The tomograms were registered on a Hamamatsu 2300x2300 pixel detector.

The reconstruction of the measured objects was done with the aid of proprietary GE software datosX ver. 2.1.0 with the use of Feldkamp algorithm for a cone beam X-ray CT [1]. The post reconstruction data treatment was performed using VGStudio Max 2.1 [2] and a free Fiji software [3] with a plugin BoneJ [4] and Voxler®3 – Golden Software [5]. All the examined specimens were scanned at 160 kV of the source voltage and 60 μA, with a rotation of the specimen of 360 degrees in 1600 steps. There was used an aluminum filter of 0.5 mm between the source and the sample. The exposure time was 500 ms and a frame averaging of 6 and image skip of 1 was applied, resulting in a scanning time of 93 minutes. The reconstructed images had a voxel size of $(6{,}2\ \mu m)^3$.

2. Example results

Both samples denoted as 501 (the variant with a cold handle) and 502 (the variant with a warm handle) underwent the same initial preparations before the final analysis. The reconstructions were denoised using a 3D median filter with the kernel size of 3x3x3, followed by the edge smoothing procedure with a 2D median filter with a 3x3 kernel. Then both samples were reoriented in a way that the origin of the referenced system is located in the middle of the vertical axe (Z axe) of the sample. The Y axe has a radial direction and coincides with the porous changes in the sample. The X axe is perpendicular to Y and Z with a direction fulfilling a clockwise reference system orientation (Fig. 1–2).

Figures 1–2 show the reconstructed surface of the samples with a visible melting zone produced during the experimental process. The topography surface shows a meaningful differences between the samples. Thesignificant changes on the surface of sample 501 were observed, the structure formed in the melting zone reminds a porous material. For the second sample (502) similar changes were observed, although they were smaller and more roughon the surface of this area. The changes on the surface have an impact on the defected area inside the samples. In Figures 3–4 both samples were presented with a transparent surface, enabling to observe not only the outer surfaces of the sample but also its interior.

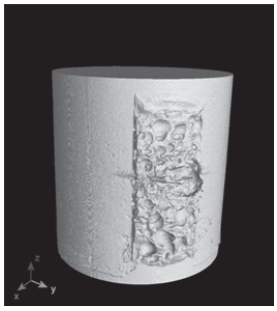

Fig. 1. Reconstructed surface of sample 501 (cold handle)

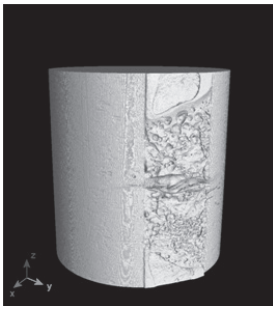

Fig. 2. Reconstructed surface of sample 502 (warm handle)

Fig. 3. Visualization of sample 501 in three spatial dimensions with transparency

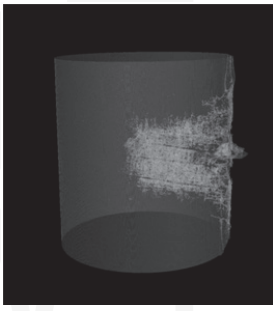

Fig. 4. Visualization of sample 502 in three spatial dimensions with transparency

The character of the pores obtained for both samples was different. In both cases, behind the melted area visible on the surface a considerable defected area occurred. Despite a much more complex surface structure of the melt in sample 501, the porous area formed behind that area is much smaller in the sense of the total volume than in the 502 sample. The pecific damage visible as bright spots on the material's surface at the bottom of the sample are observable. These are the areas of the material stratification. In a 502 sample, despite a much more extensive area with visible pores and some observable regularities in their spatial arrangement, no damageclose to the surface is observed. In both cases, the pore area ends near the sample's symmetry axis.

In the next step, a threshold value within the tomography images was selected, to separate areas filled with the material from the voids (empty areas). For this purpose, analyses of the signal intensity changes on the reconstruction images were conducted. Figure 5 presents changes for voids spaced apart from each other (solid curve) and closely located (point curve). On the basis of the curves' analysis, we decided to take the threshold value equal to 70. The reconstructed object areas with values below the threshold will be treated as voids, whereas the areas above the threshold as a solid metal.

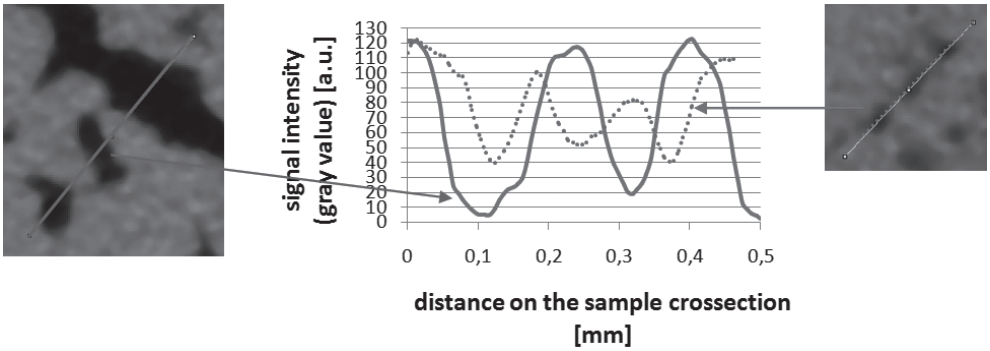

Fig. 5. Signal intensity on a sample reconstruction cross-section measured along the lines marked in a solid and points. Dark parts of the images correspond to the holes, light parts to the metal

After binarization a complex internal structure of the voids in both samples was obtained (Fig. 6a and Fig. 7a). Further analyses were based on the description of the voids within the material. For this purpose fragments belonging to the surface were removed from the

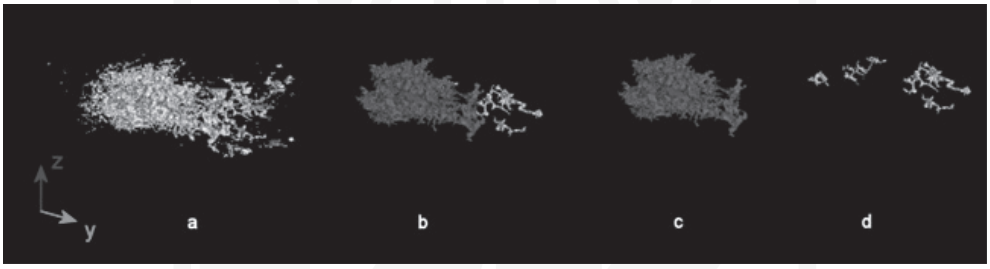

Fig. 6. Spatial structure of all voids in sample 501 (a), a large structure of the connected voids – red color, small non-interconnected voids – yellow color (b, c, d)

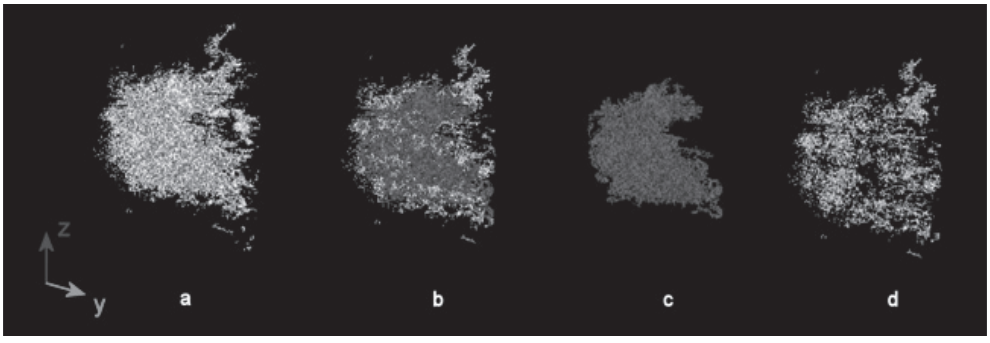

Fig. 7. Spatial structure of all voids in sample 502 (a), large structure of connected voids – red color, small non-interconnected voids – yellow color (b, c, d)

data analyzed. The analysis of the voids' continuity shows that in each sample there is only one large structure of interconnected voids and a big number of small separated voids. Visualization of the internal structures is shown in Figures 6–7. Figure 6a and Figure 7a present the spatial structure of all voids, whereas subsequent figures 6b, c, d and 7b, c, d represent a large structure of connected voids – the red color, and small separated voids – the yellow color.

To evaluate the structure's topology in both samples several parameters were calculated (detailed definitions of all parameters are given in [4] and [5]). Short descriptions of the calculated parameters are listed below. All parameters were calculated using ImageJ with Plugin BoneJ. The results were presented in Table 1:

- Volume, TV: total volume in the selected volume of interest (VOI), mm^3.
- Surface: surface area of the structure. Iso-surface constructs a triangular surface mesh by marching cubes algorithm and calculates the surface area as the sum of the areas of the triangles making up the mesh. The triangulation uses smoothing algorithms, so the sum of the surface calculated for the structure and for the holes does not have to equal the surface calculated together for the structure and holes.
- Roughness: the area of the particle divided by the volume of the particle. Low value of roughness means smoother surface. A high value of this ratio means more rugged surface.
- Mean diameter: an average diameter [mm].
- St. dev of mean diameter: standard deviation of the mean diameter of a particle.
- Maximal diameter: the diameter of the largest particle [mm].
- DA: degree of anisotropy (DA = 1 – 1/tDA), DA is 0 for isotropy and 1 for extremal anisotropy.

Table 1

Morphological parameters calculated for the examined samples

Parameter	Units	Sample 501			Sample 502		
		total	structure	holes	total	structure	holes
volume	[mm^3]	1.27	1.10	0.05	4.69	3.76	0.93
surface	[mm^2]	77	58	4	300	304	80
roughness	–	60.8	53.0	75.5	64.0	80.9	0.20
mean diameter	[mm]	0.069	0.075	0.053	0.053	0.057	0.040
st. dev. of mean diameter	[mm]	0.034	0.033	0.022	0.019	0.019	0.016
maximal diameter	[mm]	0.181	0.181	0.107	0.149	0.149	0.120
degree of anisotropy	–	0.09	0.10	1.0	0.45	0.49	0.42

Distribution of the voids' diameter is presented in Fig. 8.

In both samples a large number of unconnected voids was found. In the 501 sample, there were more than 1500 and in the 502 sample over 4500 holes. The voids, size (volume) distribution for both samples is shown in Fig. 9.

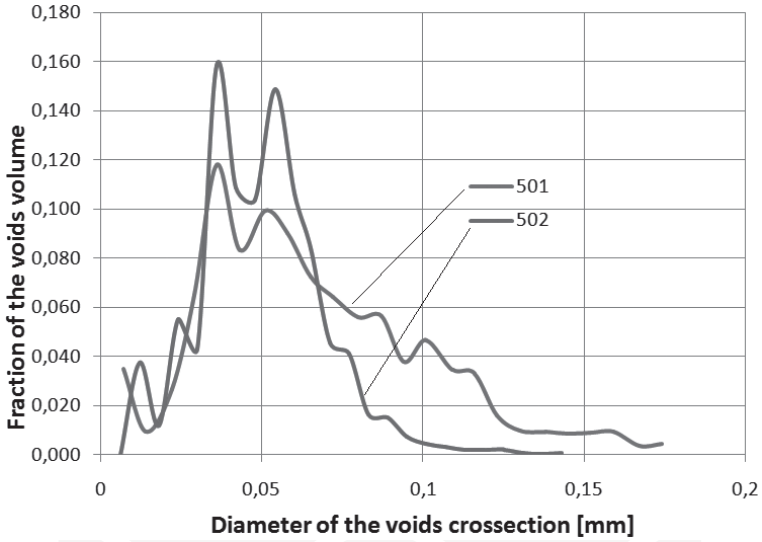

Fig. 8. Distribution of voids' diameters in both samples

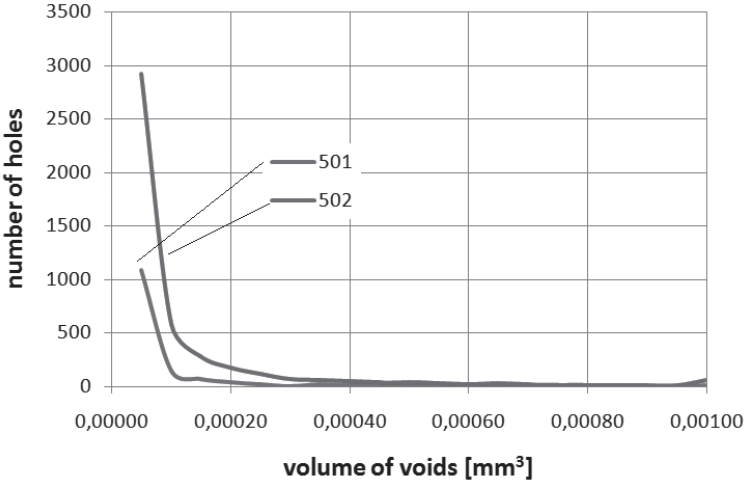

Fig. 9. Distribution of holes' volumes in both samples

For both samples the volume of the voids in each 6.25 μm thick layer, perpendicular to the sample symmetry axis, was determined. The center of the coordinate system was arbitrarily located in the position of the sample's higher porosity (close to the center of the bar). Voids' volume distribution along the sample's symmetry axis was presented in Fig. 10. Both samples have a comparable maximum porosity near the centre, but the width of the porous zone is much larger in the 501 than in the 502 sample.

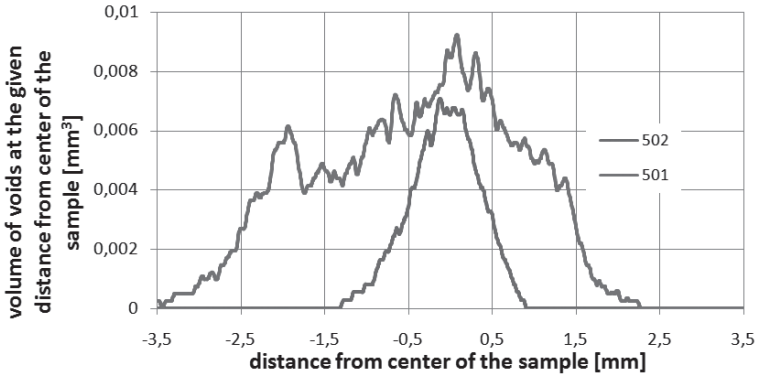

Fig. 10. Volume of the voids in the 6.25 μm layers perpendicular to the symmetry axis of the samples

In order to present the spatial distribution of coherent structures inside each sample the projections in XY, YZ and XZ planes were calculated. The results were presented in Figures 11–12. From these projections, it appears that the porous areas within the samples have a regular structure. It is especially evident for sample 502. The structure of projections on the plane shows some preferred directions, which are bar axis and the direction along the radius. It is not so clear for sample 501, but some preferred directions of slits were also observed.

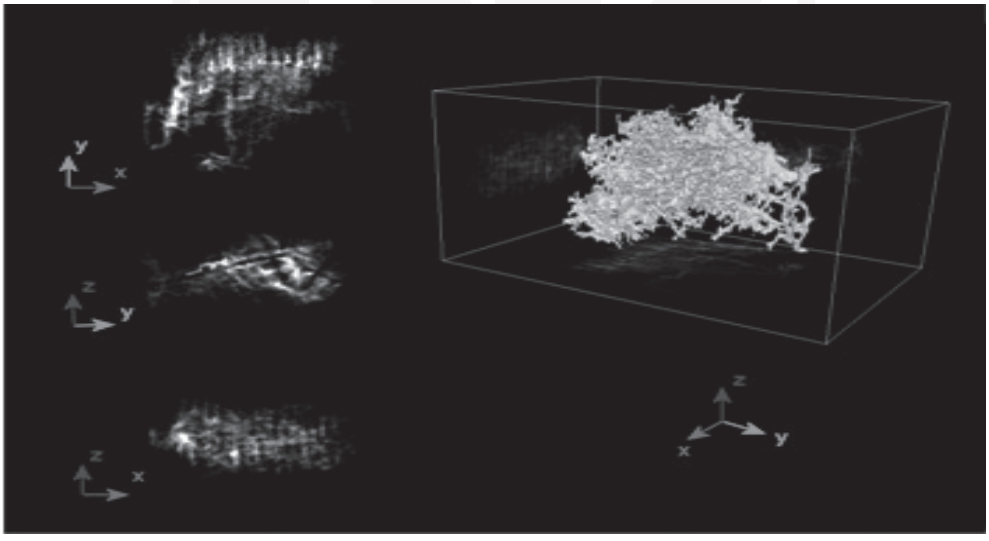

Fig. 11. The spatial distribution of coherent structures for sample 501 with the projections of these structures on the XY, YZ and XZ plane

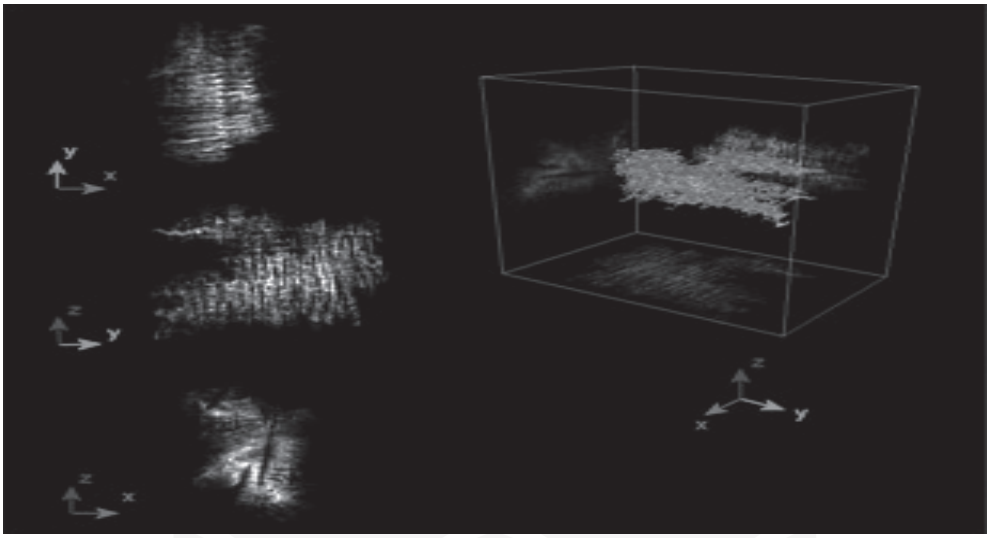

Fig. 12. The spatial distribution of coherent structures for sample 502 with the projections of these structures on the XY, YZ and XZ plane

3. Conclusions

In both samples, one coherent area of high volume joining the majority of the voids inside is observed. What is more, in each sample, there is a large number of considerably smaller, irregularly shaped voids not connected with the main structure. Elongation of the voids in both samples is similar. In each of them, about 65% of the voids have a spherical or slightly elongated character. Furthermore, approximately 8% of the voids are very or extremely elongated. The main difference between the two examined samples is the size of the voids. In sample 501 they occupy only 1.27 mm^3, and in sample 502 up to 4.69 mm^3. In both samples, the unified structure is rougher than the individual holes, which is probably due to its complex shape. The main structure of sample 501, while being smaller in terms of volume, is much larger in a mean diameter (average 75 μm compared to 53 μm in sample 502). This means that there are fewer slits in sample 501, but they are larger than in 502 sample. On the other hand, the voids within sample 501 are more condensed than in the 502 one.

The project has been supported by the Polish National Science Centre, Decision number: DEC-2011/03/D/ST8/04041.

References

[1] Feldkamp L.A., Davis L.C., Kress J.W., *Practical cone-beam algorithm*, J. Opt. Soc. Am., 1984, 612-619.
[2] Reference Manual VGStudio Max Release 2.0 (http://www.volumegraphics.com/en).
[3] http://fiji.sc/Fiji.
[4] Doube M., Kłosowski M.M., Arganda-Carreras I., Cordeliéres F., Dougherty R.P., Jackson J., Schmid B., Hutchinson J.R., Shefelbine S.J., *BoneJ: free and extensible bone image analysis in ImageJ.*, Bone, Vol. 47, 2010, 1076-1079.
[5] http://www.goldensoftware.com/products/voxler
[6] Hojny M., *Projektowanie dedykowanych systemów symulacji odkształcania stali w stanie półciekłym*, Wyd. Wzorek, 2014 (w druku).

PK